CSMA 2024
16ème Colloque National en Calcul des Structures
13-17 Mai 2024, Presqu'île de Giens (Var)

Development of high-fidelity numerical models for 3D printing of patient-specific anatomy

L. Guezou[1], A. Barbarulo[1], B. Tie[1]

[1] *Laboratoire de Mécanique Paris-Saclay (LMPS), Université Paris-Saclay, CentraleSupélec, ENS Paris-Saclay, CNRS*
{loic.guezou,andrea.barbarulo,bing.tie}@centralesupelec.fr

Abstract — This work, a part of the RHU-EndoVx project, is carried out in collaboration with the Hospital Marie Lannelongue (91). Its primary objective is to create realistic 3D-printed models of abdominal aortic aneurysms (AAA) for surgical training and rehearsals. The work involves the formulation of equations for hyperelastic material models to match the properties of the biomimetic materials used in the construction of the models, as well as the development of an optimization algorithm utilizing Proper Generalized Decomposition (PGD) to accurately simulate their behavior.
Mots clés — hyperelasticity, model reduction, optimization, biomimetic composites.

1 Introduction and context

The present work is part of the RHU-EndoVx project, which is a multi-partners project including actors in many different fields (AI, numerical simulation, 3D printing, etc.) aiming at improving the handling of aortic lesions using new technologies for fast and personalized treatment. Here, the main goal is to improve the endovascular management of complex abdominal aortic aneurysms.

The aorta is the main artery providing blood from the heart to the rest of the body. It stretches from the heart, down to the femoral and hypogastric arteries, in the pelvic area. It can be separated into 4 main sections, as shown in Figure 1a: the ascending aorta, which ascends straight out of the heart, the aortic arch, which directs it downwards, the thoracic aorta and the abdominal aorta [10] [11].

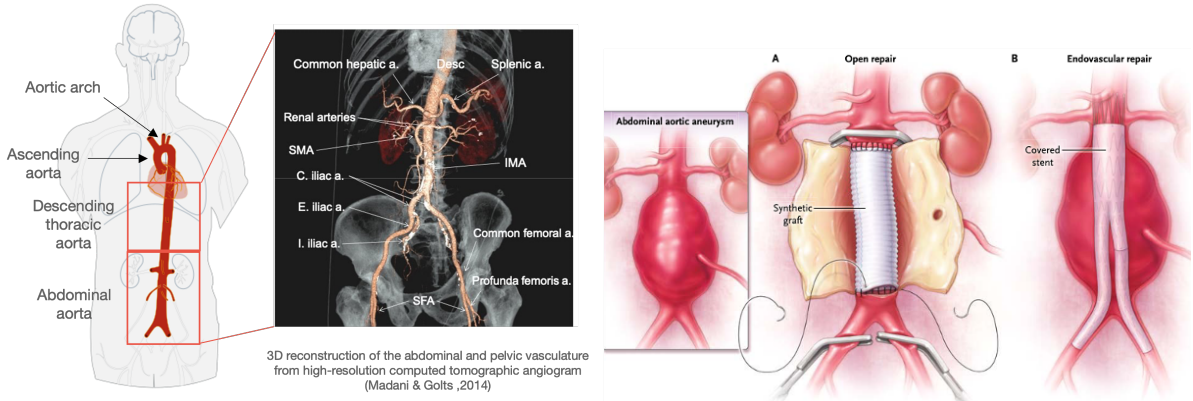

(a) (b)

Figure 1: (a) Location of the aorta in the body and 3D reconstruction [10] & (b) Open Surgery Repair (OSR) and EndoVAscular Repair (EVAR) [9]

An AAA is a permanent localized dilation of the abdominal aorta of at least 50% of the expected diameter [9]. Once detected, the treatment for an AAA is surgical repair. There are two kinds of surgeries practiced in that context: open and endovascular surgery (Figure 1b). We focus on endovascular surgery [5], as it is the more common and less dangerous surgery. Endovascular repair (EVAR) involves introducing a catheter through the femoral and iliac arteries in order to deploy a stent that will serve as a sleeve guiding the blood through the aneurysm sac, anchoring above and below the aneurysm. The operation is monitored using computed tomography angiography.

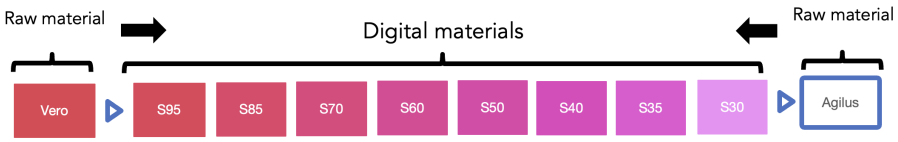

Figure 2: Diagramme showing the different raw and digital materials of the PolyJet technology [BIOMODEX™ , 2022]

This operation can be complicated and dangerous, thus it has been suggested that surgeons train in advance on a 3D-printed conformal replica of the patient's organ.

The printing technology used is the PolyJet technology, developed by the 3D printing company Stratasys™ . Droplets of UV-curable resin are jetted on a build tray using print heads and cured in a flash of UV light. This technique allows for multiple materials with varying material properties to be printed at the same time to create a final result with graded properties, such as stiffness (see [17]). In the case presented above, the materials are obtained through combinations of various degrees of Agilus and Vero, which are Stratasys™ materials (see Figure 2). These materials have a wide range of stiffnesses, from classic elasticity to hyperelasticity.

This study therefore does not consider actual biological tissue, but solely the biomimetic composite used in 3D printing the models. Thus, the more complicated aspects of the material modeling and biomechanics, such as anisotropy, or complex biological microstructures are not to be considered.

(a) (b)

Figure 3: (a) Example of a printed model in Marie Lannelongue Hospital in the operation simulation setup [Author's collection, 2022] & (b) Picture of a rupture in a printed model at the trials in Marie Lannelongue Hospital. [Author's collection, 2022]

However, in the tests carried out on printed models at Marie Lannelongue Hospital (Figure 3a), it has been shown that the current process should be improved. Indeed, the models often ruptured at unexpected and unrealistic places, such as around the bifurcations between the aorta and the iliac, femoral and hypogastric arteries (Figure 3b). These issues make it important to design a process that allows printing a working and viable model quickly.

The objectives are thus to create a layer of numerical optimization before printing, by adding appropriate mechanical modeling using, in particular, the hyperelasticity theory and efficient reduced order modeling (ROM) solvers in order to get the correct results at the first print. We write the appropriate formulations for hyperelasticity, which is the appropriate theory for biological aortic tissue, and the most flexible PolyJet materials [8]. Then, we develop the formulation of the parametric Proper Generalized Decomposition (PGD) model reduction technique, using a specific innovative algorithm taking care of the strong nonlinearity of the problem which has not been applied to such cases before in order to set the foundation for faster computation times in the rest of the project.

2 Model problem in a hyperelastic framework

This section details the base problem and material properties used in the study. We will first write the fundamental equations and derive the weak formulation from the principle of virtual works before exposing the constitutive equations of hyperelastic materials, notably taking a look at the different forms of strain energy.

2.1 Weak formulation

Let us consider an undeformed continuum body Ω, bounded by $\partial\Omega$, such that $\partial_u\Omega$ and $\partial_\sigma\Omega$ are a partition of $\partial\Omega$.

Ω is also called the initial configuration. Under the body forces $\mathbf{f}$, the prescribed boundary forces $\mathbf{g}$ and the prescribed displacement $\bar{\mathbf{u}}$, its current configuration is noted Ω_t. $\mathbf{X}$ is the position in the initial configuration, and $\mathbf{x}$ in the current (deformed) configuration, such that $\mathbf{x} = \mathbf{X} + \mathbf{u}$, with $\mathbf{u}$ the displacement that we are solving for.

Our non-linear boundary problem expresses:

$$\begin{aligned} \mathrm{Div}_{\mathbf{X}}\mathbf{P} + \mathbf{f} &= \mathbf{0} \qquad \text{on } \Omega \\ \mathbf{u} &= \bar{\mathbf{u}} \qquad \text{on } \partial_u\Omega \\ \mathbf{g} = \mathbf{P}\cdot\mathbf{n} &= \bar{\mathbf{g}} \qquad \text{on } \partial_\sigma\Omega \end{aligned} \tag{1}$$

$\mathbf{P}$ is the first Piola Kirchhoff stress tensor, ρ_0 the density of the material, $\mathbf{n}$ the unit outward normal vector. We assume the problem to be static.

Through some manipulation, one determines the weak form of the initial value boundary problem to be:

$$\mathcal{F}(\mathbf{u}, \delta\mathbf{u}) = \int_\Omega \mathbf{P} : D_{\mathbf{X}}\delta\mathbf{u} \; \mathrm{d}\Omega - \int_\Omega \mathbf{f}\cdot\delta\mathbf{u} \; \mathrm{d}\Omega - \int_{\partial_\sigma\Omega} \bar{\mathbf{g}}\cdot\delta\mathbf{u} \; \mathrm{d}\partial\Omega = 0 \tag{2}$$

$\delta\mathbf{u}$ is the virtual displacement field, used here as a test function. We have the first Piola-Kirchhoff tensor $\mathbf{P} = J\underline{\underline{\sigma}}\mathbf{F}^{-T}$, $\underline{\underline{\sigma}}$ the Cauchy stress tensor, and the second Piola-Kirchhoff stress tensor $\mathbf{S}$ such that $\mathbf{P} = \mathbf{FS}$.

Using $\delta\mathbf{E} = \mathrm{sym}(\mathbf{F}^T D_{\mathbf{X}}\delta\mathbf{u})$ the variation of the Euler-Lagrange tensor (as in [7]), the principle of virtual works with the 2nd Piola-Kirchhoff stress tensor can then be written as:

$$\mathcal{F}(\mathbf{u}, \delta\mathbf{u}) = \int_\Omega \mathbf{S} : \delta\mathbf{E} \; \mathrm{d}\Omega - \int_\Omega \mathbf{f}\cdot\delta\mathbf{u} \; \mathrm{d}\Omega - \int_{\partial_\sigma\Omega} \bar{\mathbf{g}}\cdot\delta\mathbf{u} \; \mathrm{d}\partial\Omega = 0 \tag{3}$$

A classical way to solve the problem is to linearize explicitly the weak formulation 3 and then use a Newton-Raphson scheme. In our case, it is not necessary, as the PGD algorithm we use takes care of the non-linearity in another way, as is exposed in section 3.

2.2 Constitutive equations

A hyperelastic material is a material that exhibits nonlinear elasticity and is characterized by a strain energy density function (also known as the strain energy potential or the hyperelastic material model), which characterizes how the energy of the material changes with the deformation (see [7] and [15]). These materials are essential for modeling and understanding the behavior of soft and elastomeric materials, like rubber, biological tissues, and certain types of polymers.

A common distinction among hyperelastic materials is whether the material is compressible or incompressible. This has to do with the response in the variation of the volume of the body when subjected to deformation. As expected, compressible materials see their volume change greatly when deformed, whereas incompressible materials show very little to no volume change. This has to be taken into account in the material model, meaning in the strain energy density function.

This function, or strain energy as we will call it in the rest of this paper, denoted ψ is linked to the stress tensor. It is completely determined by the constitutive equation linking stress and strain, namely

$$\mathbf{S} = \mathbb{C} : \mathbf{E} \tag{4}$$

where $\mathbb{C}$ is the modulus tensor, which is different from the classic linear elasticity Hooke tensor, $\mathbf{C} = \mathbf{F}^T\mathbf{F}$ the right Cauchy-Green tensor, $\mathbf{F} = \mathbf{I} + D_X\mathbf{u}$ the deformation gradient tensor, and $\mathbf{E} = \frac{1}{2}(\mathbf{C} - \mathbf{I})$ is the Euler-Lagrange strain tensor. Finally, $\mathbf{S}$ is the 2nd Piola-Kirchhoff stress tensor.
ψ is involved in the expression of $\mathbb{C}$. It is a function of $\mathbf{C}$, therefore it can be written as a function of $\mathbf{E}$, and its analytical formula can be obtained from the following equation.

$$\mathbf{S} = \frac{\partial \psi}{\partial \mathbf{E}} = 2\frac{\partial \psi}{\partial \mathbf{E}} \tag{5}$$
$$\psi(\mathbf{C}) = \sum_{(p,\,q)=0}^{\infty} C_{pq}(I_1(\mathbf{C}) - 3)^p (I_2(\mathbf{C}) - 3)^q$$

$\psi(\mathbf{C})$ has numerous specific forms in the literature, for compressible and incompressible materials. The most common ones are a form of Rivlin's law, as written in the second line of equation (5), where $I_i(\mathbf{C})$ $(i = 1,2,3)$ are the invariants of the Cauchy-Green right tensor.$I_1(\mathbf{C}) = \mathrm{tr}(\mathbf{C})$; $\mathrm{I}_2(\mathbf{C}) = \frac{1}{2}(\mathrm{tr}(\mathbf{C})^2 - \mathrm{tr}(\mathbf{C}^2))$; $\mathrm{I}_3(\mathbf{C}) = \det(\mathbf{C}) = \mathrm{J}(\mathbf{C})^2$. In what follows, the dependence of the invariants of $\mathbf{C}$ on $\mathbf{C}$ will be omitted to simplify the notations. The most significant Rivlin laws are the neo-Hookean, the Mooney-Rivlin and the Signorini laws.

In our study, we choose to use a Neo-Hookean model due to its simplicity (meaning $C_{20} = C_{01} = 0$). However, in the future, it will be interesting to expand our results to more models.

The incompressibility constraint for a hyperelastic material is expressed as $I_3 = 1$. In order to take it into account properly, one needs to modify the strain energy density function to $\psi = \psi(\mathbf{C}) - \frac{1}{2}p(I_3 - 1)$, where p acts as an indeterminate Lagrange multiplier.

3 Proper Generalized Decomposition of space and load position with a non-linear material model

The purpose of model order reduction is to be able to approximate a complex system with only a handful of degrees of freedom. It uses the redundancy of information available in a field, be it known or defined implicitly by a partial differential equation (PDE). To generate an accurate approximation of the original model, it projects the initial model on a low-dimensional reduced basis.

In this section, we describe the PGD and its potential use with a non-linear material model like the one described earlier. The PGD technique is an *a priori* model reduction technique relying on the separation of variables in the solution to compute quickly and efficiently the solutions to some complex problems. For instance, the most usual separation is the one of space and time for a dynamic problem.

However, the separation of other variables has also been introduced, such as the different space coordinates (x_1, x_2, x_3), or material properties. More specifically, PGD has been used in biomechanical applications, such as the real-time simulation of the haptic feedback of a liver [12] [13]. .

In this framework, we intend to conduct a parametric optimization of our models, using most notably the position of the load as a parameter. Indeed, during an EVAR, the surgeon uses guidewires and catheters inside the organ, which exerts a force whose position and amplitude vary greatly.

Using the load position as a parameter has been done using PGD on 3D formulations by Niroomandi *et al.*, both using an explicit linearization [12] and the Asymptotic Numerical Method [13] to handle the non-linear nature of hyperelastic materials. In the present work, we propose to use an innovative algorithm to take care of the nonlinearity of the problem, presented in [6]. This algorithm handles non-linearity at each stage of the PGD algorithm, using all the information about the current content of the solution instead of linearizing the general formulation first. Although it has been used previously on nonlinear thermodynamics problems and the resolution of the Navier-Stokes equation, it has never been applied to a hyperelastic material model and the nonlinearity that follows.

The following decomposition is introduced, denoting $\mathbf{u}^n(\mathbf{x}, s)$ the solution at the n^{th} iteration of the PGD solving process ($n < N_{mod}$), $\mathbf{x}$ the position of any point in the body, and s the position of the load on the boundary that is accessible to the surgeon:

$$\mathbf{u}^n(\mathbf{x}, s) = \sum_{i=1}^{n} \sum_{j=1}^{3} \phi_j^i(\mathbf{x})\ \lambda_j^i(s)\mathbf{e}_j \tag{6}$$

where $\mathbf{e}_j$ is a vector of the orthonormal basis of the 3D space. More specifically, s is a surface meshing of the portion of the boundary where loading can be applied, noted Γ_s.

Alternatively, one can write

$$\mathbf{u}^n(\mathbf{x},s) = \sum_{i=1}^{n} \boldsymbol{\phi}^i(\mathbf{x}) \circ \boldsymbol{\lambda}^i(s) \tag{7}$$

where $\phi^i(\mathbf{x}) = \sum_{j=1}^{3} \phi_j^i(\mathbf{x})\mathbf{e}_j$ and $\lambda^i(s) = \sum_{j=1}^{3} \lambda_j^i(s)\mathbf{e}_j$ are the separated fields used to approximate the displacement field $\mathbf{u}(\mathbf{x},s)$, added to i^{th} iteration of the PGD solving process, and $\circ$ is used to denote the so-called Hadamard or Schur multiplication for vectors. Then, $\boldsymbol{\phi}(\mathbf{x})$ and $\boldsymbol{\lambda}(s)$ are discretized similarly to the FEM approach, with $\mathbb{N}$ the set of interpolation functions for the space $\mathbf{x}$, and $\mathbb{N}^{\lambda}$ the one for the load position s.

$$\begin{cases} \phi_j^i(\mathbf{x}) = \mathbb{N}(\mathbf{x}) \cdot \boldsymbol{\Phi}_j^i \\ \lambda_j^i(s) = \mathbb{N}^{\lambda}(s) \cdot \boldsymbol{\Lambda}_j^i \end{cases} \tag{8}$$

In the rest of this document, $(\boldsymbol{\phi}^n(\mathbf{x}), \boldsymbol{\lambda}^n(s))$ is the couple of newly calculated separated fields to improve $\mathbf{u}_{n-1}(\mathbf{x},s)$.

Description of the PGD algorithm introduced in [6], to be used in our case

Starting from the non-linearized weak formulation of the problem 3, one applies the decomposition described in equation 6. The formulation is modified in the following way, by integrating over the domain of the parameter s in addition to the integration over the whole domain:

$$\int_{\Gamma_s}\int_{\Omega} \mathbf{S} : \delta\mathbf{E} \ \mathrm{d}\Omega \ \mathrm{d}\Gamma - \int_{\Gamma_s}\int_{\Omega} \mathbf{f} \cdot \delta\mathbf{u} \ \mathrm{d}\Omega \ \mathrm{d}\Gamma - \int_{\Gamma_s}\int_{\partial_\sigma\Omega} \bar{\mathbf{g}} \cdot \delta\mathbf{u} \ \mathrm{d}\partial\Omega \ \mathrm{d}\Gamma = 0 \tag{9}$$

Then, we need to compute N_{mod} PGD couples, or modes $(\boldsymbol{\Phi}^i, \boldsymbol{\Lambda}^i)_{(i=1,\dots,N_{mod})}$. At each iteration of computing one mode, there are two steps: an enrichment step (the actual computation of the mode) and the update stage (the re-computation of all the load position functions).

First, the enrichment step computes the modes. At iteration n, assuming all $n-1$ first modes known, one has

$$\mathbf{u}^n = \sum_{i=1}^{n} \boldsymbol{\phi}^i \circ \boldsymbol{\lambda}^i = \mathbf{u}^{n-1}(\mathbf{x},s) + \boldsymbol{\phi}^n \circ \boldsymbol{\lambda}^n \tag{10}$$

As we use the previous mode $\mathbf{u}^{n-1}$, special attention is required on the computation of the first couple $(\boldsymbol{\phi}^1, \boldsymbol{\lambda}^1)$. One needs to initialize $u(\mathbf{x},s) = u_0$ and compute the appropriate matrix operators needed in the computation of the modes using this value. We then use a fixed-point algorithm to determine the modes. After running one iteration of this algorithm to compute $(\boldsymbol{\phi}^{1,(1)}, \boldsymbol{\lambda}^{1,(1)})$ with the initialized operators (the superscript indicating the fixed-point iteration), we use it to re-calculate the operators. We repeat the operation until the convergence of this first pair $(\boldsymbol{\phi}^{1,(1)}, \boldsymbol{\lambda}^{1,(1)})$ is reached according to a relative error criterion or a maximum number of iterations.

To compute the other couples is easier and less resource-consuming. Let us consider the n^{th} couple $(\boldsymbol{\phi}^n, \boldsymbol{\lambda}^n)$. We use $\mathbf{u} = \mathbf{u}^{n-1} = \sum_{i=1}^{n-1} \boldsymbol{\phi}^i \circ \boldsymbol{\lambda}^i$ to compute and update the matrix operators. In the fixed-point algorithm, to determine the new couple, one needs to solve two problems successively and repeatedly until convergence:

- Compute $\boldsymbol{\phi}^{n,(k)}$ using the known $\boldsymbol{\lambda}^{n,(k-1)}$.
- Compute $\boldsymbol{\lambda}^{n,(k)}$ using the newly computed $\boldsymbol{\phi}^{n,(k)}$.

Then, the update stage re-computes all the load position functions $(\boldsymbol{\lambda}^i)_{i=1,\dots,n}$. At step n, as the couple $(\boldsymbol{\phi}^n, \boldsymbol{\lambda}^n)$ is now known, one computes the matrix operators using $\mathbf{u}^n(\mathbf{x},s) = \sum_{i=1}^{n} \boldsymbol{\phi}^i \circ \boldsymbol{\lambda}^i$, and uses them to re-calculate all the load position functions.

This algorithm has the particularity of treating the nonlinearity of the problem globally: the behavior law's non-linearity is dealt with over all the integration points, in the fixed-point loop for the first mode,

and right before it for the other, less energetic modes. In our hyperelastic case, the operators that are defined during this procedure become very complex and are not detailed here for the sake of legibility, compared to the quite classical operators that would appear in the linear elastic case.

PGD algorithm in pseudo-code

Here is the PGD strategy summed up in an algorithm.

Require: The non-linearized variational formulation, the material parameters, and the initializing value for displacement u_0

$\mathbf{u}(\mathbf{x},s) \leftarrow \mathbf{u_0}$
$n \leftarrow 1$ ▷ Initialization in order to count the number of modes necessary to reach convergence
Computation of the matrix operators using $\mathbf{u_0}$.
Initialization of the error criterion tolerance tol_{PGD}.
// Loop over the PGD modes
while $\varepsilon_{PGD} > tol_{PGD}$ **do** ▷ ε_{PGD} is a convergence criterion
    // Enrichment step
    if $N_{mod} = 0$ **then**
        // Fixed-point algorithm
        Initialization of the FP error criterion tolerance tol_{FP} or max number of iterations.
        Compute $\phi^{1,(1)}$ and $\lambda^{1,(1)}$ with the just initialized matrix operators.
        $k \leftarrow 2$.
        while $\varepsilon_{FP} > tol_{FP}$ **do** ▷ ε_{PGD} is a relative error criterion
            Compute $\phi^{1,(k)}$ using the known $\lambda^{1,(k-1)}$ and the matrix operators.
            Compute $\lambda^{1,(k)}$ using the just computed $\phi^{1,(k)}$ and the matrix operators.
            $k \leftarrow k+1$
            Calculate ε_{FP}.
            Recompute the matrix operators using $\mathbf{u} = (\phi^{1,(k)} \circ \lambda^{1,(k)})$.
        end while
        $\phi^1 \leftarrow \phi^{1,(k)}$; $\lambda^1 \leftarrow \lambda^{1,(k)}$
    else
        // Fixed-point algorithm
        Initialization of the FP error criterion tolerance tol_{FP}.
        Initialization of $\phi^{n,(1)}$ and $\lambda^{n,(1)}$ (for example, with ϕ^{n-1} and λ^{n-1}).
        $k \leftarrow 2$.
        Compute the matrix operators using $\mathbf{u}\left(=\sum_{i=1}^{n-1} \phi^i \circ \lambda^i\right)$.
        while $\varepsilon_{FP} > tol_{FP}$ **do** ▷ ε_{PGD} is a relative error criterion
            Compute $\phi^{n,(k)}$ using the known $\lambda^{n,(k-1)}$ and the matrix operators.
            Compute $\lambda^{n,(k)}$ using the just computed $\phi^{n,(k)}$ and the matrix operators.
            $k \leftarrow k+1$
            Calculate ε_{FP}.
        end while
        $\phi^n \leftarrow \phi^{n,(k)}$; $\lambda^n \leftarrow \lambda^{n,(k)}$
    end if
    // Update step
    Compute the matrix operators using $\mathbf{u} = \left(\sum_{i=1}^{n} \phi^i \circ \lambda^i\right)$
    Recompute all the $(\lambda^i)_{i=1,\dots,n}$
    // End of the iteration
    $\mathbf{u} \leftarrow \sum_{i=1}^{n} \phi^i \circ \lambda^i$
    $n \leftarrow n+1$
end while
$N_{mod} \leftarrow n$
return $\mathbf{u}$.

4 Conclusions

The first steps of our approach, which aims at improving the 3D printed models replicating patient-specific aneurysmal aortae, have been completed. The appropriate hyperelastic material model has been developed, and the variational formulation has been written, in both a linearized and its original non-linearized form. In order to allow for faster and more efficient computations, and in the path to the development of a full optimization method, an innovative PGD algorithm has been applied to our specific formulation, separating the physical space and the position of the load the surgeon applies on the boundary. The algorithm for this strategy of implementation of the PGD technique has been written, and the numerical implementation is a work in progress. The first results are expected to follow soon and will be presented in more detail during the conference.

Another objective of this study is to use shell theory in order to accelerate even more the computations and reduce their cost further. The combined use of shell models and PGD requires rewriting the formulations with the proper kinematics, which is the next step in our project. Such work has been done before (see [16] and [18]) with a different separation of variables.

References

1. Chinesta, F. & Cueto, E. *PGD-Based Modeling of Materials, Structures and Processes* ISBN: 978-3-319-06181-8 978-3-319-06182-5 (Springer International Publishing, 2014).
2. Chinesta, F., Cueto, E. & Huerta, A. in *Separated Representations and PGD-Based Model Reduction* (eds Chinesta, F. & Ladevèze, P.) 27–89 (Springer Vienna, 2014). ISBN: 978-3-7091-1793-4 978-3-7091-1794-1.
3. Chinesta, F. & Ladevèze, P. *PGD in Computational Mechanics: State of the Art and Prospective* Reduced Bases International WorkshopLaboratoire de Mécanique et Technologie. 2011.
4. Chinesta, F. *et al.* Towards a Framework for Non-linear Thermal Models in Shell Domains. *International Journal of Numerical Methods for Heat & Fluid Flow* **23** (ed Li, X.) 55–73. ISSN: 0961-5539 (2013).
5. Dakhlou, A. & Gaudric, J. Anévrismes de l'aorte abdominale : place du traitement chirurgical ou endovasculaire. *EM Premium.* ISSN: 0242-3960 (2016).
6. Favoretto, B., de Hillerin, C., Bettinotti, O., Oancea, V. & Barbarulo, A. Reduced Order Modeling via PGD for Highly Transient Thermal Evolutions in Additive Manufacturing. *Computer Methods in Applied Mechanics and Engineering* **349,** 405–430. ISSN: 00457825 (2019).
7. Holzapfel, G. A. *Nonlinear Solid Mechanics: A Continuum Approach for Engineering* ISBN: 978-0-471-82304-9 978-0-471-82319-3 (Wiley, 2000).
8. Holzapfel, G. A. & Ogden, R. W. *Biomechanics of Soft Tissue in Cardiovascular Systems* ISBN: 978-3-211-00455-5 978-3-7091-2736-0 (Springer Vienna, Vienna, 2003).
9. Kent, K. C. Abdominal Aortic Aneurysms. *New England Journal of Medicine* **371** (ed Solomon, C. G.) 2101–2108. ISSN: 0028-4793, 1533-4406 (2014).
10. Madani, M. M. & Golts, E. in *Reference Module in Biomedical Sciences* (Elsevier, 2014). ISBN: 978-0-12-801238-3.
11. Mercadante, A. A. & Raja, A. in (StatPearls Publishing, 2023).
12. Niroomandi, S. *et al.* Real-Time Simulation of Biological Soft Tissues: A PGD Approach: REAL-TIME SIMULATION OF BIOLOGICAL SOFT TISSUES: A PGD APPROACH. *International Journal for Numerical Methods in Biomedical Engineering* **29,** 586–600. ISSN: 20407939 (2013).
13. Niroomandi, S., Alfaro, I., González, D., Cueto, E. & Chinesta, F. Model Order Reduction in Hyperelasticity: A Proper Generalized Decomposition Approach: A PGD APPROACH FOR HYPERELASTICITY. *International Journal for Numerical Methods in Engineering* **96,** 129–149. ISSN: 00295981 (2013).

14. Nouy, A. A Priori Model Reduction through Proper Generalized Decomposition for Solving Time-Dependent Partial Differential Equations. *Computer Methods in Applied Mechanics and Engineering* **199,** 1603–1626. ISSN: 00457825 (2010).

15. Ogden, R. W. in *Biomechanics: Trends in Modeling and Simulation* (eds Holzapfel, G. A. & Ogden, R. W.) 83–156 (Springer International Publishing, 2017). ISBN: 978-3-319-41473-7 978-3-319-41475-1.

16. Prulière, E. 3D Simulation of Laminated Shell Structures Using the Proper Generalized Decomposition. *Composite Structures* **117,** 373–381. ISSN: 02638223 (2014).

17. Tee, Y. L., Peng, C., Pille, P., Leary, M. & Tran, P. PolyJet 3D Printing of Composite Materials: Experimental and Modelling Approach. *JOM* **72,** 1105–1117. ISSN: 1047-4838, 1543-1851 (3 2020).

18. Vidal, P., Gallimard, L. & Polit, O. Shell Finite Element Based on the Proper Generalized Decomposition for the Modeling of Cylindrical Composite Structures. *Computers & Structures* **132,** 1–11. ISSN: 00457949 (2014).